npj | 2D materials and applications

Article

Published in partnership with FCT NOVA with the support of E-MRS

https://doi.org/10.1038/s41699-024-00450-3

Monolayer indium selenide: an indirect bandgap material exhibits efficient brightening of dark excitons

Naomi Tabudlong Paylaga[1,2,3], Chang-Ti Chou[3], Chia-Chun Lin[1,2,3], Takashi Taniguchi[4], Kenji Watanabe[5], Raman Sankar[6], Yang-hao Chan[3,7] ✉, Shao-Yu Chen[8,9] ✉ & Wei-Hua Wang[3] ✉

Atomically thin indium selenide (InSe) exhibits a sombrero-like valence band, leading to distinctive excitonic behaviors. It is known that the indirect band gap of atomically thin InSe leads to a weak emission from the lowest-energy excitonic state (A peak). However, the A peak emission of monolayer (ML) InSe was observed to be either absent or very weak, rendering the nature of its excitonic states largely unknown. Intriguingly, we demonstrate that ML InSe exhibits pronounced PL emission because of the efficient brightening of the momentum-indirect dark excitons. The mechanism is attributed to acoustic phonon-assisted radiative recombination facilitated by strong exciton-acoustic phonon coupling and extended wavefunction in momentum space. Systematic analysis of layer-, power-, and temperature-dependent PL demonstrates that a carrier localization model can account for the asymmetric line shape of the lowest-energy excitonic emission for atomically thin InSe. Our work reveals that atomically thin InSe is a promising platform for manipulating the tightly bound dark excitons in two-dimensional semiconductor-based optoelectronic devices.

Tightly bound excitons in two-dimensional (2D) semiconductors ascribed to the reduced dielectric screening of Coulomb interactions have attracted intensive attention from the fundamental exciton science to emerging photonic and optoelectronic applications[1–5]. Bright excitons exhibit great oscillator strengths, but their ultrashort radiative lifetimes on the sub-picosecond timescale hinder potential optoelectronic and catalytic applications that require a long exciton lifetime. In contrast, dark excitons, such as spatial- and momentum-indirect excitons, have a higher population density and a longer lifetime of approximate nanoseconds; nevertheless, these excitons are optically inaccessible due to their weak coupling to light. Therefore, exploring mechanisms that can effectively brighten the dark exciton is crucial for extending the functionality of indirect gap materials[6,7].

Layered III–VI post-transition metal chalcogenides are semiconductors with distinctive optical properties, including a strong layer-dependence of the optical band gap[8–11], broad spectral response[12–14], indirect band structures[10,15,16], and strong photoresponsivity[17,18]. The band edge of atomically thin indium selenide (InSe) is considered indirect, owing to a weak inversion of the hole dispersion of the maximum-energy valence band[10,15,16,19,20]. Figure. 1a shows the electronic band structure of monolayer (ML) InSe calculated by employing GW approximation to the quasi-particle energy. The topmost valence band (v_1) has a sombrero-like band edge[10,15,16], in contrast to the lower valence bands with parabolic dispersions and band maxima at the Γ point. Next, we focus on two bright excitons and a momentum-indirect dark exciton: A and B excitons are bright excitons, consisting of electrons at the lowest conduction band (c_1) and holes at the v_1 and second-to-topmost valence band (v_2), respectively. The sombrero-like valence band leads to a most energetic-favorable and highly degenerated momentum-indirect dark excitons at the van-Hove singularity around the Γ point (marked as dark excitons in Fig. 1a), leading to intriguing optical properties in ML InSe[19]. In particular, experimental demonstrations of A exciton luminescence of ML InSe are still under debate, as recent works reported either undetectable[8,9,15] or very weak signals[10,21]. Therefore,

[1]Molecular Science Technology Program, Taiwan International Graduate Program, Academia Sinica, Taipei 10617, Taiwan. [2]National Central University, Zhongli, Taoyuan 320317, Taiwan. [3]Institute of Atomic and Molecular Sciences, Academia Sinica, Taipei 10617, Taiwan. [4]Research Center for Materials Nanoarchitectonics, National Institute for Materials Science, 1-1 Namiki, Tsukuba 305-0044, Japan. [5]Research Center for Electronic and Optical Materials, National Institute for Materials Science, 1-1 Namiki, Tsukuba 305-0044, Japan. [6]Institute of Physics, Academia Sinica, Taipei 115201, Taiwan. [7]Physics Division, National Center of Theoretical Sciences, Taipei 10617, Taiwan. [8]Center of Atomic Initiative for New Materials, National Taiwan University, Taipei 10617, Taiwan. [9]Center for Condensed Matter Sciences, National Taiwan University, Taipei 10617, Taiwan. ✉e-mail: yanghao@gate.sinica.edu.tw; shaoyuchen@ntu.edu.tw; wwang@sinica.edu.tw

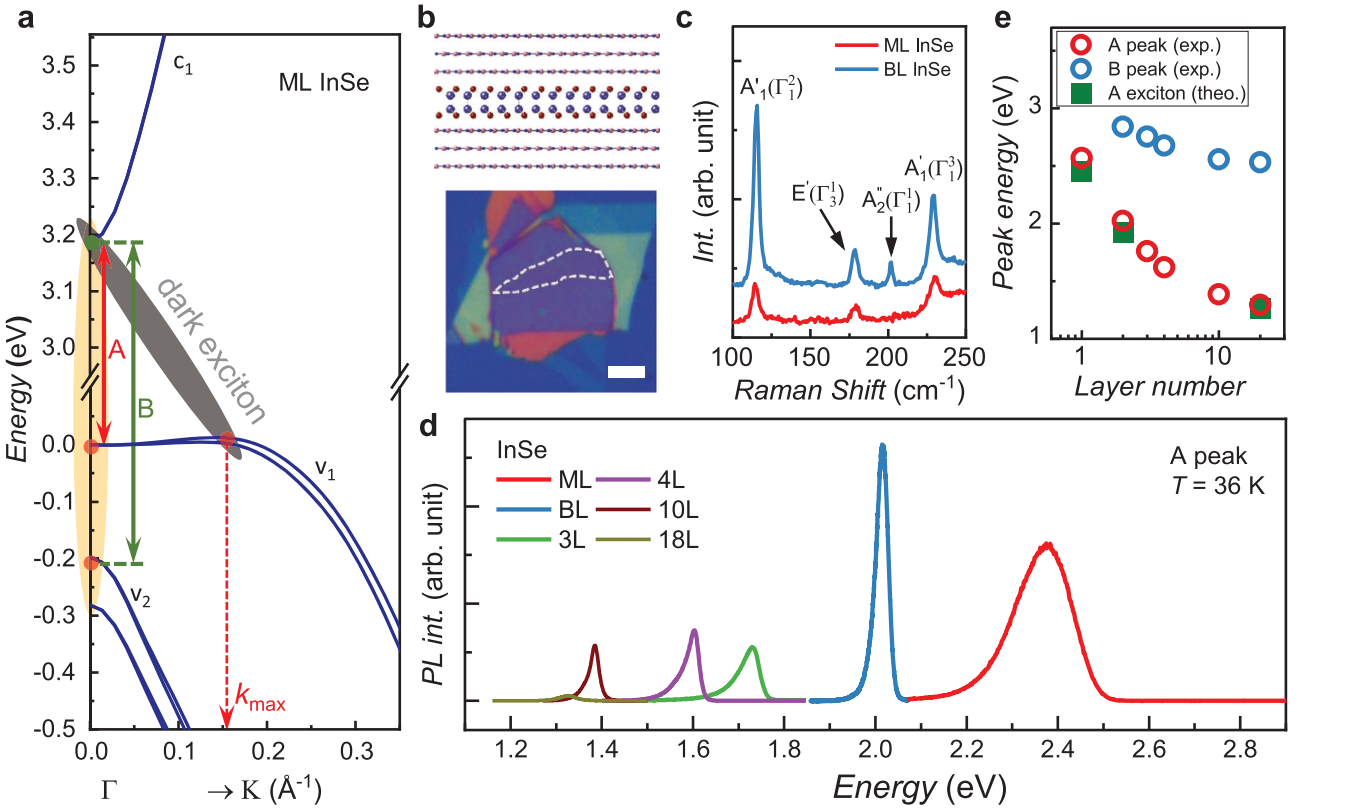

Fig. 1 | Band structures and photoluminescence spectra of atomically thin InSe. **a** Electronic band structure of ML InSe with the transition of bright A and B excitons and momentum-indirect dark exciton denoted. **b** Upper panel: Schematic of h-BN encapsulated ML InSe. Lower panel: Optical micrograph of a typical h-BN encapsulated ML InSe sample. The area of ML InSe is outlined by a white dashed line. The scale bar is 10 μm. **c** Raman spectra of the ML and BL InSe. **d** PL spectra of the A peaks of InSe from ML to 18 L. **e** Extracted PL peak energies of the A and B peaks along with the theoretically calculated excitation energies of the A excitons of ML, BL, and bulk InSe.

investigating the luminescent properties of ML InSe and understanding the excitonic behavior of the indirect excitons is essential.

In this work, we investigate the excitonic properties of atomically thin InSe by employing photoluminescence (PL) spectroscopy. We observe robust PL emission originating from a momentum-indirect dark exciton in a high-quality hexagonal boron nitride (h-BN)-encapsulated ML InSe at $T = 36$ K, despite that an indirect band structure typically leads to weak luminescence. Additionally, we detect an apparent asymmetric PL line shape in the lowest-energy emission for atomically thin InSe at cryogenic temperatures, suggesting that the long-lived dark excitons undergo carrier localization. By analyzing the PL emission with a carrier localization model, the energy of the A peak of ML InSe can be extracted as 2.58 eV, consistent with the excitation energy of the A exciton in our calculation.

Results and discussion

The γ-phase InSe crystals are grown by the Bridgman method[22]. We employ h-BN flakes to encapsulate the atomically thin InSe to ensure high sample quality. The InSe and h-BN flakes are mechanically exfoliated and stacked using the dry transfer method[23] in a nitrogen environment. An inert environment for exfoliation and stacking is essential for maintaining the crystalline quality, especially for atomically thin InSe[24,25]. Figure. 1b shows a schematic of an h-BN-encapsulated InSe and an optical micrograph of a typical h-BN-encapsulated InSe sample in upper and lower panels, respectively. The details of sample preparation and atomic force microscopy topography of the InSe sample are provided in Supplementary Note 1. The crystalline quality of h-BN-encapsulated ML and bilayer (BL) InSe is characterized by Raman spectroscopy, as shown in Fig. 1c. Notably, we observe four intrinsic Raman peaks from both ML and BL InSe at 116.1 cm^{-1}, 178.3 cm^{-1}, 199.4 cm^{-1}, and 227.1 cm^{-1}, corresponding to $A_1'(1)$, $E''(2)$, $A_2''(1)$, and $A_1'(2)$ vibrational modes[26,27], respectively, confirming their high crystalline quality.

To study the PL emission of ML InSe, we employ a cavity-stabilized diode laser at 3.05 eV as the excitation light source (Supplementary Note 1). Figure 1d shows the spectra of the lowest energy PL emission of h-BN-encapsulated InSe from ML to 18 L at $T = 36$ K. The PL energies corresponding to the lowest-energy emissions, denoted as A peaks, are in good agreement with previous reports for bulk and few-layer InSe[9,28]. The layer dependence of the A peaks significantly blueshift with decreasing thickness due to the quantum confinement effect[8–10,21,29]. Intriguingly, we observe the pronounced A peak of ML InSe. Moreover, in addition to A peaks, we observe distinct PL emissions from B excitons at higher energy regimes, denoted hereafter as B peaks, down to BL InSe (Supplementary Note 2), highlighting the ultrawide spectral response from 1.3 eV to 2.9 eV of InSe from ML to bulk. Figure 1e summarizes the PL energies of the A and B peaks for atomically thin and bulk InSe, as well as calculated excitation energies of A excitons for ML, BL, and bulk InSe. The calculation detail of the absorption spectra is described in Supplementary Note 3. The energies of the A peaks for ML, BL, and bulk InSe coincide well with the calculated transition energies, strongly substantiating the assignment of the A peak of ML InSe.

Figure 1d further reveals the layer dependence of the PL intensities: ML and BL InSe manifest pronounced PL of A peak, and the PL intensity generally decreases with the increasing number of layers. Due to the in-plane mirror symmetry of InSe, the A transition from in-plane photoexcitation associated with the s to the p_z orbitals is prohibited. However, spin-orbit coupling (SOC) can mix the p_x, p_y and p_z orbitals, enabling A exciton to couple to in-plane polarized light[30]. This SOC strength increases with decreasing thickness, rendering a maximum effect in ML InSe[30]. It is noted that in our measurement setup with the objective lens in the out-of-plane

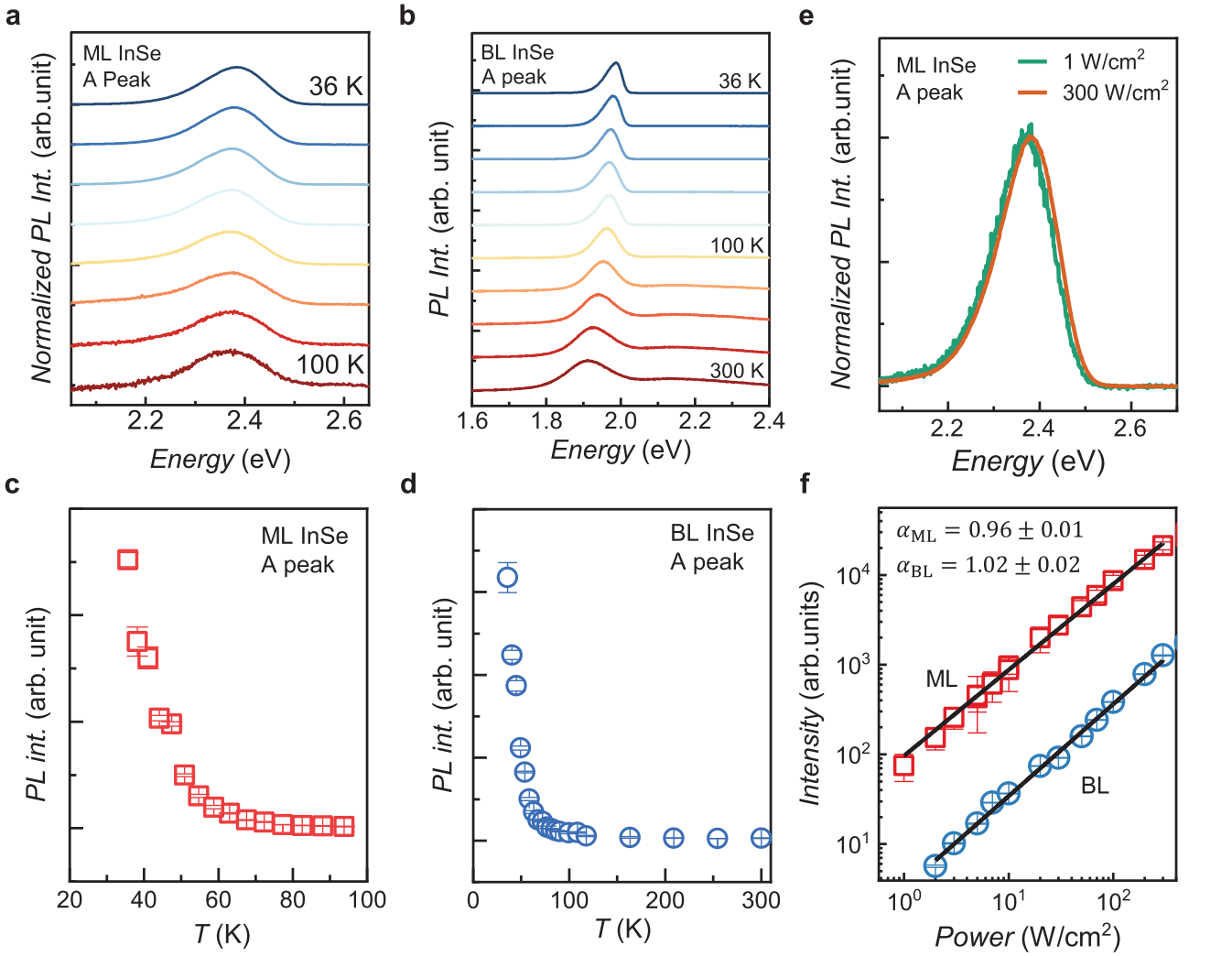

Fig. 2 | Excitonic properties of atomically thin InSe. a, **b** The normalized PL spectra of ML and BL InSe at different temperatures. The PL spectra are shifted vertically for clarity. **c**, **d** The temperature dependence of PL intensity of A peak of ML and BL InSe. **e** Normalized PL spectra of ML InSe taken at 1 W/cm^2 and 300 W/cm^2. **f** Excitation power dependence of PL intensities of the A peaks of ML and BL InSe. The black line shows the linear power law fittings, yielding exponents α_{ML} and α_{BL} to be very close to unity for ML and BL InSe.

direction, the in-plane polarized light is effectively collected from the samples, facilitating the detection of A peak emission from ML InSe.

The PL of indirect transition governed by phonon-assisted processes is typically weak. The pronounced luminescence from A peak of ML InSe suggests the strong exciton-phonon coupling that efficiently brightens the dark exciton. Figure 2a, b plot the T-dependent PL spectra for ML and BL InSe, respectively. The observed PL peak continuously evolves from $T = 36$ K up to higher T, indicating that same type of exciton is involved. Figure 2c, d show the T dependence of the integral intensity of A peak of ML and BL InSe, respectively, revealing a monotonic increase with decreasing T. Such T dependence has been reported for the indirect PL emission in the studies of other 2D semiconductors[31,32]. At $T = 36$ K, absorbing LA phonons in ML InSe can efficiently upconvert the dark excitons to the bright A exciton state because of matching momentum and energy. However, phonons can also lead to non-radiative recombination, competing with the radiative processes. Our results suggest that the non-radiative recombination becomes dominant at higher T range, resulting in suppression of the PL intensity with increasing T.

In Figure. 2e, we compare the normalized PL spectra of the A peak of ML InSe with the excitation powers of 1 W/cm^2 and 300 W/cm^2. The PL line shape is almost identical over an excitation power range of more than two orders of magnitude. In addition, we observe no additional emission at the low energy side, which can be associated with other mechanisms, such as biexcitonic recombination, secondary radiative recombination, and defect-bound excitonic states[33,34]. ML InSe exhibits a small blueshift, which can be attributed to state filling of the photoexcited carriers[35–37]. We plot the power dependence of the PL intensities of the A peaks of ML and BL InSe in Fig. 2f. The PL intensities of both ML and BL InSe can be well-described by a power law of the exponent of 0.96 and 1.02. We thus can rule out that the observed PL emission of ML and BL InSe is due to defect-bound excitons or biexcitons because they exhibit a sublinear[33] or superlinear power law[34,38], respectively.

Next, we discuss the spectral line shape of PL emission and its indication of the excitonic properties of the atomically thin InSe. Figure 3a plots the normalized PL spectra from the A peaks of ML to 18 L InSe to emphasize the evolution of line shapes. A peak of ML to 10 L InSe exhibits asymmetric line shapes with low-energy tails and steep high-energy shoulders. In contrast, the A peak of 18 L and B peaks (detailed in Supplementary Note 2) are symmetric. To analyze these asymmetric line shapes of the A peaks, we employ a carrier localization model[39], as depicted in Fig. 3b, c. This model accounts for a spatial fluctuating potential, leading to a random distribution of surface potential energy. This potential fluctuation in the conduction and valence bands causes spatial variations in exciton energy. We consider two competing processes of exciton dynamics: (1) carrier localization, where

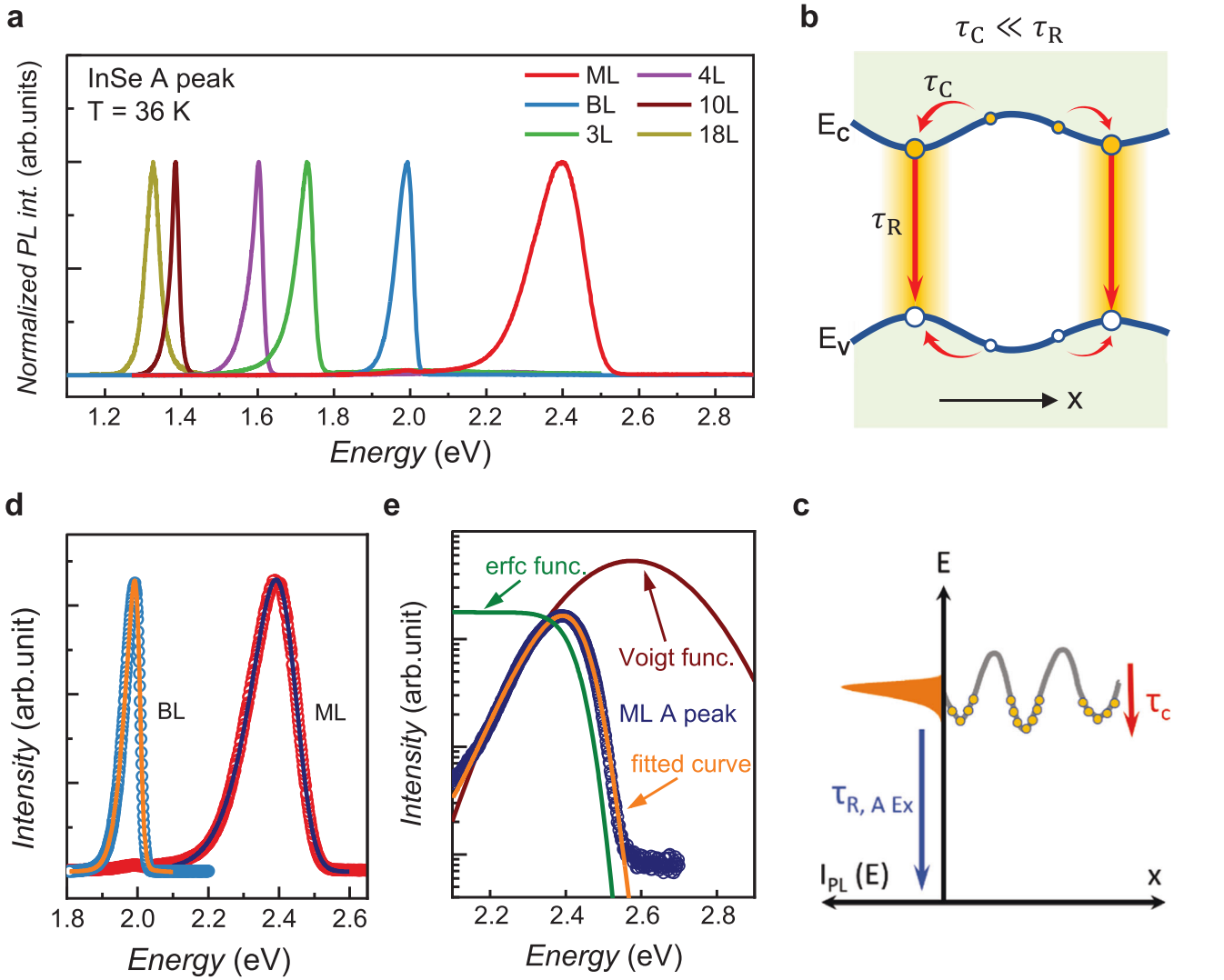

Fig. 3 | PL line shape analysis of atomically thin InSe and carrier localization model. a Normalized PL spectra of the A peaks of InSe from ML to 18 L. **b** Schematic of the carrier localization model when the carrier localization time is smaller than the recombination time. **c** PL spectra of the A peaks of ML and BL InSe are fitted by the carrier localization model. **d** Asymmetric PL line shape of ML InSe and various functions employed for fitting. **e** A schematic diagram depicts the presence of potential fluctuations-induced energy redistribution and the asymmetric line shape.

photoexcited electrons and holes migrate to local energy minima (characteristic time ~ τ_C) and (2) exciton radiative recombination (radiative recombination time ~ τ_R). Here, all other decay paths of photoexcited electrons and holes are assumed to be negligible.

Quantitatively, in the carrier localization model, the PL line shape can be described by the following equation[39]:

$$I(E) = y_0 + I_0(E)exp\left\{\frac{-\tau_R}{2\tau_C}\left(erfc\left(\frac{E_{exc}-E}{\sqrt{2}\sigma_E}\right)\right)\right\} \quad (1)$$

where E_{exc} is the exciton peak energy, σ_E is the average potential fluctuations energy, and $I_0(E)$ is the exciton population function. We approximate $I_0(E)$ by a Voigt function[40,41], which consists of the contributions of homogeneous (w_L) and inhomogeneous broadening (w_G) with Lorentzian and Gaussian forms, respectively. The Voigt function can be written as

$$I_0(E) = A\frac{2ln2}{\pi^{3/2}}\frac{w_L}{w_G^2}\int_{-\infty}^{\infty}\frac{e^{-t^2}}{\left(\sqrt{ln2}\frac{w_L}{w_G}\right)^2+\left(\sqrt{4ln2}\frac{x-x_c}{w_G}-t\right)^2}dt \quad (2)$$

where x_c is the peak center. There are 5 free parameters in the Voigt-based carrier localization model, including $E_{exc}, \sigma_E, w_L, w_G, and\ \tau_R/\tau_C$. As shown in Fig. 3d, the PL spectra of the A peaks for ML and BL InSe are well-fitted, validating the carrier localization model to account for the asymmetric PL line shape.

Figure 3e shows the fitting results of PL spectra of ML InSe along with the corresponding Voigt and error functions in log scale. Without carrier localization ($\tau_C \gg \tau_R$, the excitonic PL emission exhibits typically symmetric line shape. However, for atomically thin InSe, the excitonic ground state is momentum-indirect, leading to a much longer radiative lifetime than bright excitons with a direct band gap. For ML InSe, the dark excitons are characterized by a long radiative recombination lifetime; τ_R is estimated to be on the order of 10 ns (Supplementary Note 4). Also, previous time-resolved PL measurements had shown a long radiative lifetime of 8 ns for few-layer InSe[28], suggesting that τ_R may significantly greater than τ_C. Under such conditions, the carrier localization effect takes place: Higher energy excitons migrate to lower energy sites before direct recombination, leading to suppressed exciton recombination at the high-energy side, as illustrated in Fig. 3b, c. The energy redistribution is observable through the PL line shape, providing valuable insights into the excitonic behavior in atomically thin

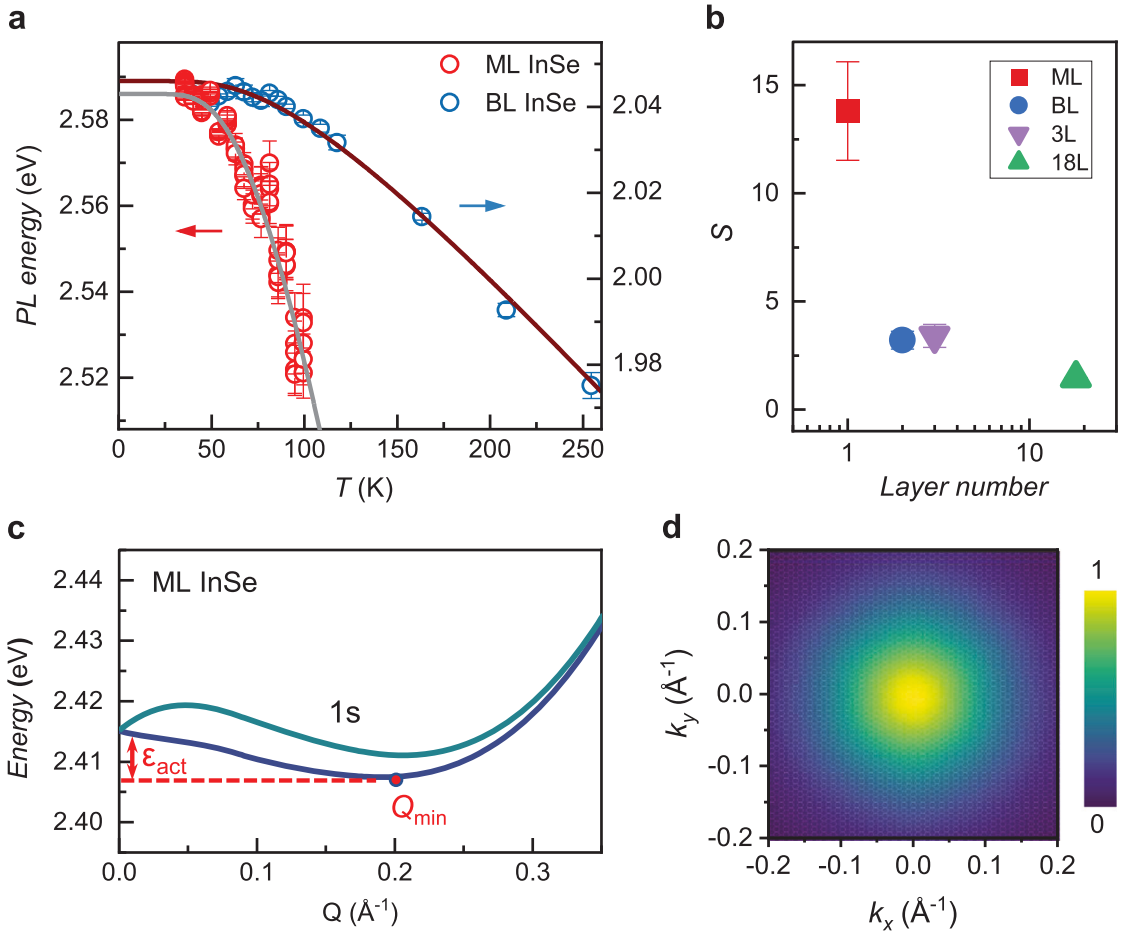

Fig. 4 | Strong exciton-phonon coupling and brightening of the indirect excitons of ML InSe. a Temperature dependence of the PL peak energies of the A peaks of ML and BL InSe. The solid curves are fitted by O'Donnell-Chen model as described in Eq. (3). **b** Extracted exciton-phonon coupling strengths of ML, BL, 3 L, and 18 L InSe, showing an enhancement trend with a decreasing layer number and strong exciton-phonon coupling for ML InSe. **c** Exciton dispersion of ML InSe showing the two low excitonic bands associated with the A exciton at $Q = 0$. **d** Envelope function of the A exciton of ML InSe in momentum space.

InSe layers. Significantly, our fitting results of the asymmetric PL emission support the long τ_R of the momentum-indirect dark excitons in atomically thin InSe.

We note that the carrier localization model is not exclusive to excitons but is equally applicable to other quasiparticles, for instance trions and biexcitons, in 2D semiconductors that exhibit a similar interplay of different recombination processes. This is particularly relevant in atomically thin 2D materials, where the potential fluctuations in the atomic layers are greatly susceptible to extrinsic effect due to a weak dielectric screening and a substantial surface-to-volume ratio. Nonetheless, it is noted that the carrier localization effect becomes negligible when τ_R is substantially shorter than τ_C. For excitons with short τ_R, such as bright excitons, and 2D materials with uniform potential energy and thus long τ_C, the carrier localization model become no longer applicable.

To assess the role of phonons participating in the luminescence, we extract the PL peak energy for ML and BL InSe as a function of temperature (T) using carrier localization model, as shown in Fig. 4a. While the PL peak positions of both ML and BL InSe show a monotonically decreasing trend, ML InSe manifests a stronger T dependence compared with BL InSe. The sample temperature is calibrated to quantitatively access the phonon effect (Supplementary Note 5). The T-dependent PL peak energy can be described by O'Donnell-Chen model[42–44]:

$$E_G(T) = E_G(0) - SE_{ph}\left[\coth\left(\frac{E_{ph}}{2k_BT}\right) - 1\right] \quad (3)$$

where $E_G(0)$ represents the optical band gap at $T = 0$ K, S is a dimensionless constant associated with the strength of exciton-phonon coupling, and E_{ph} is the average phonon energy. The ML and BL InSe data are well described by this equation, yielding $S = 14$ and $S = 3$ and $E_{ph} = 23.5$ meV and 23.1 meV for ML and BL InSe, respectively. Figure 4b plots the S values for ML, BL, 3 L, and 18 L InSe; The fitting parameters are summarized in Supplementary Note 6. Our results show a distinct enhancement of S as the thickness of InSe decreases, with a significantly large S for ML InSe. The large exciton-phonon coupling strength of ML InSe can be attributed to strong scattering of hole in ML InSe by longitudinal acoustic (LA) phonons at the sombrero-like valence band maximum, in contrast to much weaker LA scattering for BL and bulk InSe[45]. Moreover, electrons in ML InSe is subjected to large scattering from the longitudinal optical (LO) phonons, compared with the one in bulk InSe[45], further enhancing the exciton-phonon coupling. In addition, strong electron-phonon coupling in ML InSe has also been attributed to a large deformation potential resulting from heavy holes[46] or a combination of strong piezoelectric properties and a lack of inversion symmetry[47].

The phonon-assisted brightening of the indirect dark excitons is further examined by considering the exciton band structure in ML InSe. We calculate the exciton dispersion of ML InSe, and the two lowest-energy bands associated with bright A excitons are shown in Fig. 4c. The first band exhibits an energy minimum at Q_{min} 0.2 Å^{-1}, originating from the weakly inverted, topmost valence band, as shown in Fig. 1a. The weakly inverted valence band is attributed to the vanishing momentum matrix element between the topmost valence band and the lowest conduction band from

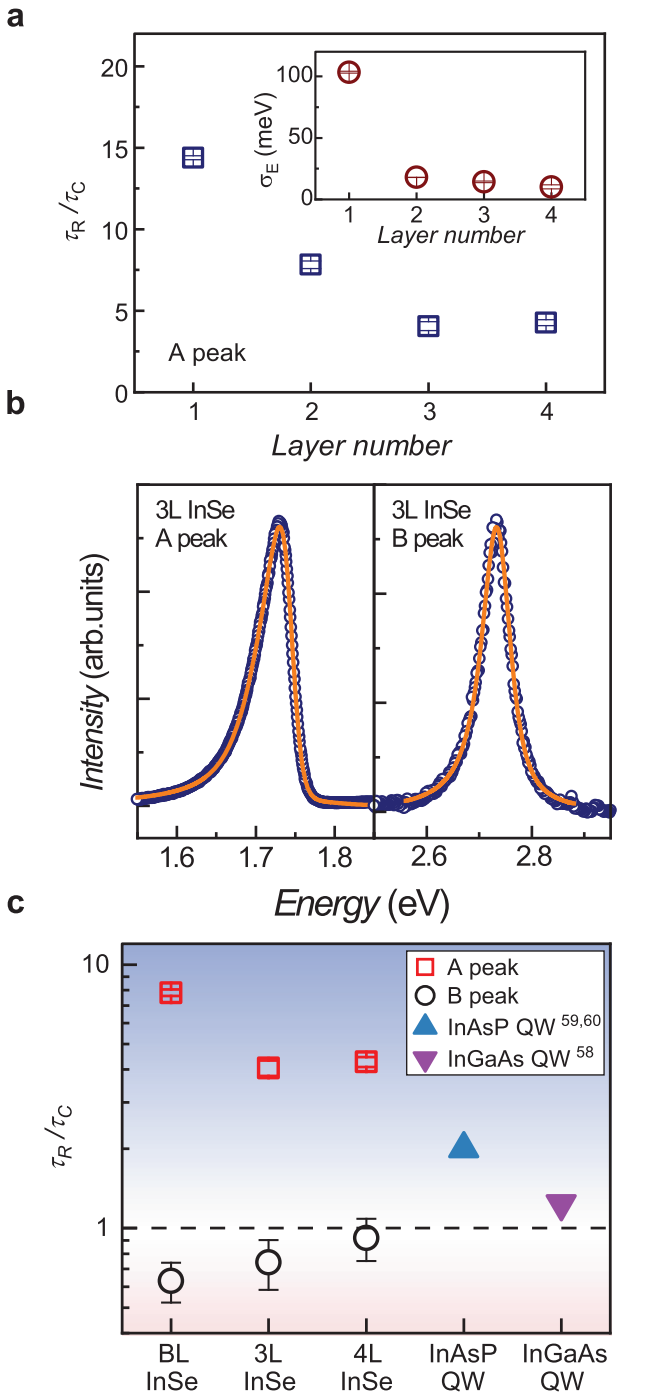

Fig. 5 | Comparison of the A and B peaks of atomically thin InSe and the carrier localization model. a Extracted τ_R/τ_C from ML to 4 L InSe at $T = 36$ K. Inset: the extracted average potential fluctuations energies of atomically thin InSe from ML to 4 L. **b** PL spectra of the A and B peaks of 3 L InSe and the fitting curves by the carrier localization model. **c** Comparison of the τ_R/τ_C extracted from the A and B peaks of atomically thin InSe from BL to 4 L and other quantum wells composed of compound semiconductors.

$k \cdot p$ theory[48]. The dark exciton at the lowest energy, denoted as the $k_{max}\Gamma$ exciton, consists of the hole located at the k_{max} and the electron at the Γ valley. From the exciton dispersion, the corresponding activation energy (ε_{act}) is defined as the energy difference between the optically active state at $Q = 0$ and the Q_{min} exciton state. ML InSe exhibits a very small ε_{act} of 8 meV, which is easily susceptible to excitation, leading to highly probable phonon-assisted emission. For a tightly bound exciton in real space with a tiny Bohr radius, its exciton distribution greatly extends in momentum space[49], which can enhance exciton-phonon coupling. To be quantitative, we calculate the A exciton envelop function of ML InSe, as shown in Fig. 4d. The exciton envelope function ranges well beyond k 0.15 Å^{-1} from the Γ point, signifying a large overlap with the lowest-energy bands of bright A excitons at $Q = 0$, facilitating efficient phonon-assisted radiative recombination. It is noted that the aforementioned strong exciton-phonon coupling of ML InSe favors a hot phonon effect[50–52]. Moreover, from the calculated LA phonon of ML InSe, a dispersion of approximately 7 meV with k 0.3 Å^{-1} along the Γ-K direction[45,52,53] can provide the needed energy and momentum to activate the momentum-indirect $k_{max}\Gamma$ exciton through acoustic phonon absorption.

Finally, we discuss the carrier localization effects in InSe with different number of layers. Figure 5a compares the τ_R/τ_C of the A peak from ML to 4 L InSe. All the τ_R/τ_C for the A peaks are larger than unity, substantiating the dominance of carrier localization in the relaxation path $\tau_C < \tau_R$ (Supplementary Note 7). Moreover, the τ_R/τ_C increases with decreasing thickness up to τ_R/τ_C 14 for ML InSe. The inset of Fig. 5a shows the extracted average potential fluctuations energy (σ_E) of ML to 4 L InSe, revealing that σ_E increases with decreasing layer number. Because of reduced screening in thinner 2D materials, the larger σ_E may be associated with the shorter τ_C of thinner InSe, which can account for the layer number dependence of the τ_R/τ_C. We note that the σ_E of ML InSe is approximately 100 meV, which is comparable to the dielectric disorder resulting from variation in the dielectric screening of h-BN and scattered polymer residue[54].

The dominance of carrier localization effects on A peak is due to the long lifetime. Figure 5b shows the PL spectra of the A and B peaks for the 3 L InSe sample. As discussed above, the asymmetric line shape of the A peaks of 3 L InSe suggests that carrier localization dominates the recombination path. We found that the PL of the B peaks of 3 L InSe exhibits much less asymmetry, which can also be well-fitted with the carrier localization model. Figure 5c compares the layer dependence of τ_R/τ_C for the A and B peaks of 2–4 L InSe, signifying that the τ_R/τ_C of the A peaks is larger than that of the B peaks. It is noted that τ_C for the A and B peaks of the same InSe sample should be similar because the localization time is determined by the magnitude of the potential fluctuation and is insensitive to the band structure. In other words, τ_R becomes the determining factor to govern the value of τ_R/τ_C in the A and B peaks. Because the A peak PL emission arises from the momentum-indirect exciton that exhibits a much longer lifetime, it can be inferred that A peak exhibits a larger τ_R/τ_C as shown in Fig. 5a, leading to different extents of asymmetry for the A and B peaks as shown in Fig. 5b.

In Fig. 5c, we further compare the observed τ_R/τ_C values with those of other material systems to which the carrier localization model is applied[39,55–57]. Generally, when $\tau_C < \tau_R$ is valid and carrier localization is the dominant relaxation path, the carrier migration is relatively fast, signifying a high diffusion coefficient. For InSe, the relatively large diffusion coefficient (~10 cm^2/s) and high carrier mobility[58] thus favor the carrier localization effect. We found that the A peaks of ML and BL InSe exhibit much higher τ_R/τ_C than quantum wells composed of compound semiconductors[39,55–57], suggesting the distinct properties of the potential fluctuation and carrier recombination associated with the tightly bound indirect excitons of 2D semiconductors.

In addition to the carrier localization model, we note that the virtual phonon relaxation process[32] with multiple phonon scattering cannot be completely excluded to explain the asymmetric PL line shape. However, the carrier localization model with the Voigt function for exciton population is found to comprehensively account for the extended layer-, temperature-, and power-dependent PL spectra of atomically thin InSe, hence justifies our choice of the fitting model.

In conclusion, the PL of high-quality, h-BN-encapsulated InSe samples, ranging from ML to bulk, is systematically measured and analyzed. Notably, we observe strong PL emission from the A peak of ML InSe, although its band structure suggests a dark exciton. The brightening of the momentum-indirect exciton of ML InSe can be attributed to the phonon-assisted process facilitated by the strong exciton-phonon coupling and the

extended wave function in momentum space. Furthermore, atomically thin InSe exhibits an apparent asymmetric PL for A peaks, which can be well accounted for by the carrier localization model with spatial potential fluctuation. We demonstrate the distinct excitonic behaviors, including a strong exciton-phonon coupling, a long exciton lifetime, and a large binding energy coexisting in the ML III-VI metal chalcogenides. In the context of the emerging interest in the excitonic physics of 2D semiconductors, our results pave the way for developing dark-exciton-mediated energy harvesting, quantum catalysts, and optoelectronics.

Methods

Sample fabrication

Bottom h-BN flakes were mechanically exfoliated on 300 nm SiO_2/n-Si substrates. The polymer residue from the tape was removed by annealing in a furnace at 500 °C in Ar/O_2 mixed gas. The InSe flakes were mechanically exfoliated on a PDMS gel film in a glovebox in a nitrogen environment and then transferred to the bottom h-BN through the dry transfer method. To complete the structure, h-BN flakes on PDMS were transferred onto the InSe/h-BN stacking with careful alignment to ensure encapsulation.

Optical spectroscopy measurements

The samples were mounted in a Janis (ST-500) cryostat maintained at a high vacuum (5×10^{-6} Torr). The photoexcitation was performed with a custom-built cavity-stabilized diode laser with a wavelength of 407 nm. We employ fused-silica optics to reduce the residual luminescence from glassy optics. We employed a 50x objective lens (NA: 0.5) to focus the laser to a spot size of approximately ~1 μm on the sample and to collect the PL signal under back-scattering geometry. The collected signal was directed to a Horiba iHR 550 spectrometer and then dispersed with reflective grating (150 lines/mm or 600 lines/mm for PL; 1800 lines/mm for Raman spectroscopy) and detected by the liquid-nitrogen cooled charge-coupled device of Horiba Symphony II detection system. An additional 537 nm longpass filter was added to the collection path during the measurement of the bulk A transition PL to prevent signal mixing from the B transition overtone. The Raman spectroscopy is performed with a diode-pumped solid-state laser with an energy of 2.33 eV.

Data availability

All data supporting the findings of this study are included in the paper and its Supplementary Information files. The corresponding author can also provide additional data upon reasonable request.

Received: 21 August 2023; Accepted: 8 February 2024;
Published online: 20 February 2024

References

1. Wilson, N. P., Yao, W., Shan, J. & Xu, X. D. Excitons and emergent quantum phenomena in stacked 2D semiconductors. *Nature* **599**, 383–392 (2021).
2. Mueller, T. & Malic, E. Exciton physics and device application of two-dimensional transition metal dichalcogenide semiconductors. *Npj 2d Mater. Appl.* **2**, 29 (2018).
3. Gao, S. Y., Liu, L., Wen, B. & Zhang, X. Monolayer InSe photodetector with strong anisotropy and surface-bound excitons. *Phys. Chem. Chem. Phys.* **23**, 6075–6083 (2021).
4. Zhou, J. D. et al. InSe monolayer: synthesis, structure and ultra-high second-harmonic generation. *2d Mater.* **5**, 025019 (2018).
5. Cai, Y. Q., Zhang, G. & Zhang, Y. W. Charge transfer and functionalization of monolayer InSe by physisorption of small molecules for gas sensing. *J. Phys. Chem. C.* **121**, 10182–10193 (2017).
6. Feierabend, M., Berghauser, G., Knorr, A. & Malic, E. Proposal for dark exciton based chemical sensors. *Nat. Commun.* **8**, 14776 (2017).
7. Malic, E. et al. Dark excitons in transition metal dichalcogenides. *Phys. Rev. Mater.* **2**, 014002 (2018).
8. Mudd, G. W. et al. Tuning the bandgap of exfoliated InSe nanosheets by quantum confinement. *Adv. Mater.* **25**, 5714–5718 (2013).
9. Bandurin, D. A. et al. High electron mobility, quantum Hall effect and anomalous optical response in atomically thin InSe. *Nat. Nanotechnol.* **12**, 223–227 (2017).
10. Hamer, M. J. et al. Indirect to direct gap crossover in two-dimensional InSe revealed by angle-resolved photoemission spectroscopy. *Acs Nano* **13**, 2136–2142 (2019).
11. Jung, C. S. et al. Red-to-ultraviolet emission tuning of two-dimensional gallium sulfide/selenide. *Acs Nano* **9**, 9585–9593 (2015).
12. Mudd, G. W. et al. High broad-band photoresponsivity of mechanically formed InSe-graphene van der waals heterostructures. *Adv. Mater.* **27**, 3760–3766 (2015).
13. Tamalampudi, S. R. et al. High performance and bendable few-layered InSe photodetectors with broad spectral response. *Nano Lett.* **14**, 2800–2806 (2014).
14. Yan, F. G. et al. Fast, multicolor photodetection with graphene-contacted p-GaSe/n-InSe van der Waals heterostructures. *Nanotechnology* **28**, 27LT01 (2017).
15. Mudd, G. W. et al. The direct-to-indirect band gap crossover in two-dimensional van der Waals Indium Selenide crystals. *Sci. Rep.-Uk* **6**, 39619 (2016).
16. Magorrian, S. J., Zolyomi, V. & Fal'ko, V. I. Electronic and optical properties of two-dimensional InSe from a DFT-parametrized tight-binding model. *Phys. Rev. B* **94**, 245431 (2016).
17. Lei, S. D. et al. Evolution of the electronic band structure and efficient photo-detection in atomic layers of InSe. *Acs Nano* **8**, 1263–1272 (2014).
18. Liu, F. C. et al. High-sensitivity photodetectors based on multilayer GaTe flakes. *Acs Nano* **8**, 752–760 (2014).
19. Ceferino, A., Song, K. W., Magorrian, S. J., Zolyomi, V. & Fal'ko, V. I. Crossover from weakly indirect to direct excitons in atomically thin films of InSe. *Phys. Rev. B* **101**, 245432 (2020).
20. Guo, Y. Z. & Robertson, J. Band structure, band offsets, substitutional doping, and Schottky barriers of bulk and monolayer InSe. *Phys. Rev. Mater.* **1**, 044004 (2017).
21. Brotons-Gisbert, M. et al. Nanotexturing to enhance photoluminescent response of atomically thin indium selenide with highly tunable band gap. *Nano Lett.* **16**, 3221–3229 (2016).
22. Likforman, A., Carre, D., Etienne, J. & Bachet, B. Crystal-structure of indium monoselenide (Inse). *Acta Crystallogr. B.* **31**, 1252–1254 (1975).
23. Castellanos-Gomez, A. et al. Deterministic transfer of two-dimensional materials by all-dry viscoelastic stamping. *2d Mater.* **1**, 011002 (2014).
24. Cao, Y. et al. Quality heterostructures from two-dimensional crystals unstable in air by their assembly in inert atmosphere. *Nano Lett.* **15**, 4914–4921 (2015).
25. Cheng, C. Y. et al. Phase modulation of self-gating in ionic liquid-functionalized InSe field-effect transistors. *Nano Lett.* **22**, 2270–2276 (2022).
26. Sanchez-Royo, J. F. et al. Electronic structure, optical properties, and lattice dynamics in atomically thin indium selenide flakes. *Nano Res.* **7**, 1556–1568 (2014).
27. Molas, M. R. et al. Raman spectroscopy of GaSe and InSe post-transition metal chalcogenides layers. *Faraday Discuss* **227**, 163–170 (2021).
28. Venanzi, T. et al. Photoluminescence dynamics in few-layer InSe. *Phys. Rev. Mater.* **4**, 044001 (2020).
29. Mudd, G. W. et al. Quantum confined acceptors and donors in InSe nanosheets. *Appl. Phys. Lett.* **105**, 221909 (2014).
30. Magorrian, S. J., Zolyomi, V. & Fal'ko, V. I. Spin-orbit coupling, optical transitions, and spin pumping in monolayer and few-layer InSe. *Phys. Rev. B* **96**, 195428 (2017).

31. Golovynskyi, S. et al. Exciton and trion in few-layer MoS2: thickness- and temperature-dependent photoluminescence. *Appl. Surf. Sci.* **515**, 146033 (2020).
32. Brem, S. et al. Phonon-assisted photoluminescence from indirect excitons in monolayers of transition-metal dichalcogenides. *Nano Lett.* **20**, 2849–2856 (2020).
33. Tongay, S. et al. Defects activated photoluminescence in two-dimensional semiconductors: interplay between bound, charged, and free excitons. *Sci. Rep.-Uk* **3**, 2657 (2013).
34. You, Y. M. et al. Observation of biexcitons in monolayer WSe2. *Nat. Phys.* **11**, 477–U138 (2015).
35. Chichibu, S., Azuhata, T., Sota, T. & Nakamura, S. Luminescences from localized states in InGaN epilayers. *Appl. Phys. Lett.* **70**, 2822–2824 (1997).
36. Eliseev, P. G., Perlin, P., Lee, J. Y. & Osinski, M. "Blue" temperature-induced shift and band-tail emission in InGaN-based light sources. *Appl. Phys. Lett.* **71**, 569–571 (1997).
37. Wang, Y. et al. Photoluminescence study of the interface fluctuation effect for InGaAs/InAlAs/InP single quantum well with different thickness. *Nanoscale Res. Lett.* **12**, 229 (2017).
38. Chen, S. Y., Goldstein, T., Taniguchi, T., Watanabe, K. & Yan, J. Coulomb-bound four- and five-particle intervalley states in an atomically-thin semiconductor. *Nat. Commun.* **9**, 3717 (2018).
39. Schubert, E. F. & Tsang, W. T. Photoluminescence line-shape of excitons in alloy semiconductors. *Phys. Rev. B* **34**, 2991–2994 (1986).
40. Koirala, S., Mouri, S., Miyauchi, Y. & Matsuda, K. Homogeneous linewidth broadening and exciton dephasing mechanism in MoTe2. *Phys. Rev. B* **93**, 075411 (2016).
41. Ajayi, O. A. et al. Approaching the intrinsic photoluminescence linewidth in transition metal dichalcogenide monolayers. *2d Mater.* **4**, 031011 (2017).
42. Odonnell, K. P. & Chen, X. Temperature-dependence of semiconductor band-gaps. *Appl. Phys. Lett.* **58**, 2924–2926 (1991).
43. Cadiz, F. et al. Excitonic linewidth approaching the homogeneous limit in MoS2-based van der Waals heterostructures. *Phys. Rev. X* **7**, 021026 (2017).
44. Helmrich, S. et al. Exciton-phonon coupling in mono- and bilayer MoTe2. *2d Mater.* **5**, 045007 (2018).
45. Li, W. B., Ponce, S. & Giustino, F. Dimensional crossover in the carrier mobility of two-dimensional semiconductors: the case of InSe. *Nano Lett.* **19**, 1774–1781 (2019).
46. Lee, J., Koteles, E. S. & Vassell, M. O. Luminescence linewidths of excitons in GaAs quantum-wells below 150-K. *Phys. Rev. B* **33**, 5512–5516 (1986).
47. Gopalan, S., Gaddemane, G., Van de Put, M. L. & Fischetti, M. V. Monte Carlo study of electronic transport in monolayer InSe. *Materials* **12**, 4210 (2019).
48. Rybkovskiy, D. V., Osadchy, A. V. & Obraztsova, E. D. Transition from parabolic to ring-shaped valence band maximum in few-layer GaS, GaSe, and InSe. *Phys. Rev. B* **90**, 235302 (2014).
49. Chen, S. Y. et al. Luminescent emission of excited Rydberg excitons from monolayer WSe2. *Nano Lett.* **19**, 2464–2471 (2019).
50. Herrfurth, O., Kruger, E., Blaurock, S., Krautscheid, H. & Grundmann, M. Hot-phonon effects in photo-excited wide-bandgap semiconductors. *J. Phys.-Condens Mat.* **33**, 205701 (2021).
51. Rössler, U. *Solid state theory: an introduction*. (Springer, 2004).
52. Lugovskoi, A. V., Katsnelson, M. I. & Rudenko, A. N. Strong electron-phonon coupling and its influence on the transport and optical properties of hole-doped single-layer InSe. *Phys. Rev. Lett.* **123**, 176401 (2019).
53. Pandey, T., Parker, D. S. & Lindsay, L. Ab initio phonon thermal transport in monolayer InSe, GaSe, GaS, and alloys. *Nanotechnology* **28**, 455706 (2017).
54. Raja, A. et al. Dielectric disorder in two-dimensional materials. *Nat. Nanotechnol.* **14**, 832 (2019).
55. Trifonov, A. V. et al. Nontrivial relaxation dynamics of excitons in high-quality InGaAs/GaAs quantum wells. *Phys. Rev. B* **91**, 115307 (2015).
56. Vashisht, G., Dixit, V. K., Haldar, S. & Sharma, T. K. Effect of disorders on the optical properties of excitons in InAsP/InP quantum wells investigated by magneto-photoluminescence spectroscopy. *J. Opt. Soc. Am. B.* **35**, 2405–2411 (2018).
57. Merritt, T. R. et al. Photoluminescence lineshape and dynamics of localized excitonic transitions in InAsP epitaxial layers. *J. Appl. Phys.* **115**, 193503 (2014).
58. Zhong, C. M. et al. Hot carrier and surface recombination dynamics in layered InSe crystals. *J. Phys. Chem. Lett.* **10**, 493–499 (2019).

Acknowledgements

Y.-h.C. thanks Dr. Jiawei Ruan for insightful discussions. K.W. and T.T. acknowledge support from the JSPS KAKENHI (Grant Numbers 20H00354, 21H05233 and 23H02052) and World Premier International Research Center Initiative (WPI), MEXT, Japan. This work was supported by the National Science and Technology Council of Taiwan through Grant Nos. 110-2112-M-001-065-MY3 (R.S.), 110-2124-M-002-012 (Y.-h.C.), 111-2112-M-002-047 and 112-2628-M-002-008 (S.-Y.C.), and 109-2112-M-001-041-MY3 (W.-H.W.). Y.-h.C. acknowledges support by National Center for High-Performance Computing in Taiwan. S.-Y.C. acknowledges support from the Center of Atomic Initiative for New Materials, National Taiwan University (Grant No. 111 L9008, 112 L9008, and 113 L9008) and from the Featured Areas Research Center Program within the framework of the Higher Education Sprout Project by the Ministry of Education of Taiwan.

Author contributions

N.T.P., S.-Y.C., and W.-H.W. conceived and designed this project. N.T.P. fabricated the devices with assistance from C.-C.L. S.-Y.C. constructed the PL and Raman spectroscopy measurement setup. N.T.P. and S.-Y.C. performed the optical measurements. N.T.P., S.-Y.C., and W.-H.W. performed data analysis. K.W. and T.T. provided the h-BN crystals. R.S. provided InSe crystals. C.-T.C., J.R., and Y.-h.C. performed theoretical modeling and calculations. The manuscript was written through the contributions of all authors. All authors have approved the final version of the manuscript.

Competing interests

The authors declare no competing interests.

Additional information

Supplementary information The online version contains supplementary material available at https://doi.org/10.1038/s41699-024-00450-3.

Correspondence and requests for materials should be addressed to Yang-hao Chan, Shao-Yu Chen or Wei-Hua Wang.